CETUP-2023-022, FERMILAB-PUB-24-0317-T, IPPP/24/35

Pseudo-Dirac Neutrinos and Relic Neutrino Matter Effect on the High-energy Neutrino Flavor Composition

P. S. Bhupal Dev,[1,*] Pedro A. N. Machado,[2,†] and Ivan Martínez-Soler[3,‡]

[1] *Department of Physics and McDonnell Center for the Space Sciences, Washington University, St. Louis, MO 63130, USA*
[2] *Theoretical Physics Department, Fermilab, P.O. Box 500, Batavia, IL 60510, USA*
[3] *Institute for Particle Physics Phenomenology, Durham University, South Road, DH1 3LE, Durham, UK*

We show that if neutrinos are pseudo-Dirac, they can potentially affect the flavor ratio predictions for the high-energy astrophysical neutrino flux observed by IceCube. In this context, we point out a novel matter effect induced by the cosmic neutrino background (CνB) on the flavor ratio composition. Specifically, the active-sterile neutrino oscillations over the astrophysical baseline lead to an energy-dependent flavor ratio at Earth due to the CνB matter effect, which is distinguishable from the vacuum oscillation effect, provided there is a local CνB overdensity. Considering the projected precision of the 3-neutrino oscillation parameter measurements and improved flavor triangle measurements, we show that the next-generation neutrino telescopes, such as IceCube-Gen2 and KM3NeT, can probe the pseudo-Dirac neutrino hypothesis in a distinctive way.

I. INTRODUCTION

Despite great progress in neutrino physics over the past decades, the nature of neutrino mass remains unknown. Neutrinos could be either Majorana or Dirac particles. Or they could be somewhere in-between, namely, pseudo-Dirac [1–5], which are fundamentally Majorana fermions, but behave like Dirac particles in laboratory experiments because of the extremely small mass-squared splitting (δm^2) between the active and sterile components. The theoretical and model-building aspects of pseudo-Dirac neutrinos have been extensively discussed in the literature; see e.g., Refs. [6–16]. In fact, in any model where the neutrinos start as Dirac particles with naturally small masses could actually receive quantum gravity corrections making them pseudo-Dirac particles at a more fundamental level. These corrections will generate small δm^2 via higher-dimensional operators suppressed by the Planck scale. It is interesting to note that certain string landscape (swampland) constructions also predict pseudo-Dirac neutrinos [17–20]. Small δm^2 values could also be linked to the observed baryon asymmetry of the Universe [13, 21]. Recently, the pseudo-Dirac neutrinos were also shown to resolve the excess radio background issue [22, 23].

Irrespective of the theoretical motivations, the only experimental way to directly probe the active-sterile oscillations of pseudo-Dirac neutrinos with tiny mass splittings is by going to extremely long baselines, which is possible with astrophysical sources of neutrinos, such as solar [24–30], supernova [31, 32], high-energy astrophysical [14, 16, 33–40], or relic neutrinos [41]. In fact, stringent upper limits on $\delta m^2_{1,2} \lesssim 10^{-12}$ eV^2 have been derived using the solar neutrino data [26, 29]. These limits are derived assuming the usual maximal active-sterile neutrino mixing in the pseudo-Dirac scenario. If the mixing is non-maximal, the δm^2 limits can be much weaker [42]. Moreover, the solar neutrino data is not sensitive to δm^2_3 due to the smallness of θ_{13}, and the limit from atmospheric, accelerator and reactor neutrino data is rather weak, $\delta m^2_3 \lesssim 10^{-5}$ eV^2 [27], due to the much shorter baselines. There also exists an old limit on $\delta m^2_i \lesssim 10^{-8}$ eV^2 for maximal mixing from Big Bang Nucleosynthesis considerations [43, 44].

The recent identification of a few point sources for astrophysical neutrinos [45] allowed us to set the first IceCube limits on the pseudo-Dirac neutrino hypothesis in the $\delta m^2_i \in [10^{-21}, 10^{-16}]$ eV^2 range [16]; see also Refs. [46, 47] for related analyses. However, these studies only used the IceCube track-like sample (mostly involving muon neutrinos, with a small fraction coming from tau-induced tracks), and hence, were insensitive to the full neutrino flavor information. This is justifiable because the track events have excellent angular resolution of $\lesssim 0.2^\circ$ [48] and are therefore ideal for point source identification [49], unlike the cascade events which have a poor angular resolution of $\sim 10^\circ$–15° at IceCube [50]. The cascade resolution will significantly improve up to 1.5° at KM3NeT [51] with their current high-energy cascade reconstruction algorithm, and even sub-degree resolution can be achieved with better reconstruction algorithms using the timing information and elongation emission profile of cascades [52].

In this paper, we study how including the cascade events can give us additional information on the pseudo-Dirac neutrino hypothesis. In particular, we show that the flavor ratio measurements of high-energy neutrinos, from either diffuse or point sources, would be affected in the presence of pseudo-Dirac neutrinos, except for the special case when all three active-sterile mass splittings are exactly the same. Given the fact that the flavor ratio measurements are expected to improve significantly [53] with the next-generation neutrino telescopes, such as

* bdev@wustl.edu
† pmachado@fnal.gov
‡ ivan.j.martinez-soler@durham.ac.uk

IceCube-Gen 2 [54], KM3NeT [51], Baikal-GVD [55], P-ONE [56], TRIDENT [57], TAMBO [58], Trinity [59] and RET [60], they will provide an unprecedented opportunity to test the pseudo-Dirac neutrino hypothesis.

The final flavor ratio measured on Earth crucially depends on the initial source flavor composition which is currently unknown. We take this into account by considering different well-motivated choices for $(\nu_e : \nu_\mu : \nu_\tau)$ at the source,[1] namely, (i) $(1/3 : 2/3 : 0)$ for the standard pion and muon decay [63]; (ii) $(0 : 1 : 0)$ for the muon damped case [64–68]; (iii) $(1 : 0 : 0)$ for neutron decay [69, 70]; and (iv) $(x : 1-x : 0)$ with $x \in [0, 1]$ for the general case corresponding to a mixture of multiple processes/sources contributing to the neutrino flux. In each case, we compare the expectations from the standard 3-neutrino oscillation paradigm with the pseudo-Dirac scenario for a given δm^2 to see whether they can be distinguished from each other on the flavor triangle. Note that since we are dealing with flavor ratios, we are insensitive to uncertainties related to the normalization or energy dependence of the astrophysical neutrino flux.

Moreover, for the δm^2 values of interest here, we show that the matter effect due to the cosmic neutrino background (CνB) can play an important role in determining the flavor ratios on Earth, depending on the value of the local CνB overdensity. This is in contrast with the pure vacuum oscillations assumed so far in the vast literature of flavor ratio studies (see e.g., Refs. [39, 40, 53, 71–77]).[2] This is because only the left-handed component of the pseudo-Dirac neutrino actively interacts via standard weak interactions, whereas the right-handed component is sterile. Thus, the neutral-current interactions of the left-handed component of the high-energy neutrino flux with the CνB bath would induce a difference in the matter potential for a given flavor (depending on which $\delta m_i^2 \neq 0$), which could modify the oscillation probabilities, and could even induce an MSW resonance [79, 80] for suitable values of δm_i^2. This is unlike the standard 3-neutrino case where the neutral-current interaction equally affects all three flavors and does not lead to a matter potential difference between different flavors. The same is true if all three active-sterile mass splittings δm_i^2 are the same, in which case there is no matter potential difference induced by CνB either. Thus, including the CνB matter effect would provide an additional handle on probing small δm_i^2 values at neutrino telescopes. Moreover, the matter effect introduces a novel energy-dependent flavor transition, which will help us disentangle the pseudo-Dirac scenario.

The rest of the paper is organized as follows: In Section II, we review the standard 3-flavor oscillation paradigm for the flavor triangle analysis. In Section III, we present the pseudo-Dirac case with oscillations in vacuum and in matter, but in a time-independent background. In Section IV, we discuss the CνB matter effect in an expanding Universe. In Section V, we include the CνB overdensity and the finite cluster size effect. Our results are given in Section VI. We conclude with some final remarks in Section VII.

II. STANDARD CASE

In the standard 3-neutrino oscillation scenario, the neutrino flavor eigenstates $|\nu_\alpha\rangle$, with $\alpha = e, \mu, \tau$, are related to the mass eigenstates $|\nu_i\rangle$, with $i = 1, 2, 3$, via a unitary transformation, i.e.

$$|\nu_\alpha\rangle = \sum_{i=1}^{3} U_{\alpha i}^* |\nu_i\rangle \,, \tag{1}$$

where U is the 3×3 Pontecorvo-Maki-Nakagawa-Sakata (PMNS) lepton mixing matrix, parameterized in terms of three mixing angles θ_{ij} and a Dirac CP phase $\delta_{\rm CP}$ [81].[3]

The characteristic neutrino oscillation length scale in vacuum is given by

$$L_{\rm osc}^{\rm std} = \frac{4\pi E_\nu}{\Delta m_{ij}^2} \simeq 8 \times 10^{-6} {\rm pc} \left(\frac{E_\nu}{1\ {\rm TeV}}\right) \left(\frac{10^{-5}\ {\rm eV}^2}{\Delta m_{ij}^2}\right) , \tag{2}$$

where $E_\nu \gg m_i$ is the neutrino energy and $\Delta m_{ij}^2 \equiv |m_i^2 - m_j^2|$ are the mass-squared differences. From this equation, it is clear that for high-energy neutrinos, $L_{\rm osc}$ corresponding to either solar or atmospheric mass-squared splitting is much smaller than the typical distance ($\gtrsim$ Mpc) to the extragalactic astrophysical sources. Therefore, the standard 3-neutrino oscillations are rapid enough to average out over astrophysical baselines, and we are only sensitive to the averaged out $\nu_\alpha \to \nu_\beta$ flavor transition probability,

$$P_{\alpha\beta}^{\rm std} = \sum_{i=1}^{3} |U_{\alpha i}|^2 |U_{\beta i}|^2 \,, \tag{3}$$

which depends on the 3-neutrino mixing angles, as well as on the Dirac CP phase to a lesser extent. When drawing the allowed regions in the flavor triangles, we will use the best-fit and 68% confidence level (CL) allowed values

[1] Since IceCube cannot distinguish between neutrinos and antineutrinos on an event-by-event basis (with the exception of the Glashow resonance [61] for which we lack statistics [62]), we take the sum of neutrinos and antineutrinos for a given flavor.

[2] The effect of source matter effect on the flavor composition of high-energy neutrinos from active galactic nuclei was recently considered in Ref. [78], but this becomes important only for heavily Compton-thick sources with column density $\gtrsim 10^{30}$ cm^{-2} whose exact population or contribution to the observed flux at IceCube is currently unknown.

[3] If neutrinos are Majorana, U contains two additional phases which however do not affect oscillations.

of the oscillation parameters from the recent NuFit 5.3 global fit [82, 83], assuming a normal mass ordering for concreteness. Note that the latest oscillation results from T2K [84] and NOνA [85] individually continue to show a mild preference for normal mass ordering, although their combination prefers inverted mass ordering [86], so this is still an open question.

Thus, for a given initial flavor composition at the source $(f_e, f_\mu, f_\tau)_{\rm S}$, the final flavor composition at Earth under standard vacuum oscillations is given by

$$f_{\beta,\oplus} = \sum_{\alpha=e,\mu,\tau} P^{\rm std}_{\alpha\beta} f_{\alpha,{\rm S}}\,, \tag{4}$$

where we have normalized the flavor ratios so that they add up to unity, i.e., $\sum_\alpha f_{\alpha,{\rm S}} = \sum_\beta f_{\beta,\oplus} = 1$. Depending on the physical scenario for the initial source flavor composition, we can then calculate the final flavor composition at Earth using Eq. (4). This will be referred to as the "standard case" in the following.

III. PSEUDO-DIRAC CASE

Pseudo-Dirac neutrinos can be considered as three pairs of almost degenerate mass eigenstates. The Hamiltonian describing the neutrino evolution in vacuum is given by $H^{\rm PD}_{\rm vac} = \widetilde{U}^\dagger M^2_{\rm diag}\widetilde{U}/2E_\nu$, where the masses can be separated into two sub-block 3×3 diagonal matrices $M^2_{\rm diag} = \{m^2_{iS}, m^2_{iA}\}$, with the squared mass eigenvalues

$$m^2_{iS} = m^2_i + \delta m^2_i/2\,, \tag{5}$$
$$m^2_{iA} = m^2_i - \delta m^2_i/2\,, \tag{6}$$

corresponding to the mass eigenstates

$$\nu_{iS} = \sin\theta_i \nu_{ia} + \cos\theta_i \nu_{is}\,, \tag{7}$$
$$\nu_{iA} = -i(\cos\theta_i \nu_{ia} - \sin\theta_i \nu_{is})\,, \tag{8}$$

with ν_{ia} and ν_{is} being the active and sterile components, respectively. In the case of pseudo-Dirac states, a maximal mixing between ν_S and ν_A states is assumed, i.e., $\theta_i = \pi/4$, in which case the states coincide with the symmetric $(\nu_S = (\nu_a + \nu_s)/\sqrt{2})$ and anti-symmetric $(\nu_A = -i(\nu_a - \nu_s)/\sqrt{2})$ combinations of the active and sterile components. Therefore, the mixing matrix is given by

$$\widetilde{U} = \frac{1}{\sqrt{2}}\begin{pmatrix} U & 0_{3\times3} \\ 0_{3\times3} & U_R \end{pmatrix}\begin{pmatrix} 1_{3\times3} & i_{3\times3} \\ 1_{3\times3} & -i_{3\times3} \end{pmatrix}, \tag{9}$$

where U is the PMNS matrix and U_R is the mixing matrix between the right-handed (sterile) states.

The interactions of high-energy neutrinos with the CνB introduce a matter potential, given by $\widehat{V}_\nu = V_\nu {\rm diag}\{1_{3\times3}, 0_{3\times3}\}$,[4] where $V_\nu = G_F n_\nu/\sqrt{2}$, with n_ν being the CνB number density and G_F being the Fermi constant. To diagonalize the new Hamiltonian $H^{\rm PD}_{\rm mat} = H^{\rm PD}_{\rm vac} + \widehat{V}_\nu$ in the presence of the matter potential for the pseudo-Dirac case, we notice that $\widehat{V}_\nu$ commutes with both U and U_R. Therefore, we can use three rotation matrices, one for each pair of degenerate states. The effective mixing angle in matter is given by

$$\tan 2\widetilde{\theta}_i = \frac{\delta m^2_i \sin(2\theta_i)}{\delta m^2_i \cos(2\theta_i) - A} \simeq -\frac{\delta m^2_i}{A}\,, \tag{10}$$

where $A = 2E_\nu V_\nu$. Note that for non-maximal mixing, the standard Mikheyev-Smirnov-Wolfenstein (MSW) resonance condition [79, 80] would have been obtained when $A = \delta m^2_i \cos(2\theta)$. But in the pseudo-Dirac case with maximal mixing to start with, the matter effect tends to take the effective mixing angle away from the maximal value of $\pi/4$, as shown in Eq. (10).

According to the ΛCDM model of cosmology, the CνB number density today is given by

$$n_{\nu,0} = \frac{3}{4}\frac{\zeta(3)}{\pi^2} g_\nu T^3_{\nu,0} \simeq 112\ {\rm cm}^{-3} \tag{11}$$

per neutrino flavor and the same for antineutrinos. Here $T_{\nu,0} = (4/11)^{1/3} T_{\gamma,0} \simeq 1.7\times10^{-4}$ eV is the CνB temperature and $g_\nu = 2$ is the number of degrees of freedom for each pseudo-Dirac neutrino. This gives a tiny matter potential $V_\nu \simeq 7.4\times10^{-36}$ eV which, however, becomes relevant for $\delta m^2 \gtrsim 2E_\nu V_\nu \simeq 1.5\times10^{-23}$ eV $(E_\nu/1$ TeV).

In the presence of CνB matter effect, the eigenvalues $(\lambda_{iS}, \lambda_{iA})$ of the diagonal matrix $M^2_{\rm diag}$ are given by

$$\lambda_{iS} = \frac{A}{2}\cos 2\widetilde{\theta}_i + m^2_i + \frac{\delta m^2_i}{2}\sin 2\widetilde{\theta}_i\,, \tag{12}$$
$$\lambda_{iA} = -\frac{A}{2}\cos 2\widetilde{\theta}_i + m^2_i - \frac{\delta m^2_i}{2}\sin 2\widetilde{\theta}_i\,. \tag{13}$$

In the limit when the matter potential is negligible, i.e. $A \ll \delta m^2_i$, we recover maximal mixing between active and sterile neutrinos: $\widetilde{\theta}_i \to \pi/4$ [cf. Eq. (10)] and the usual eigenvalues $\lambda_{iS} = m^2_{i1} + \delta m^2_i/2$ and $\lambda_{iA} = m^2_{i1} - \delta m^2_i/2$ [cf. Eqs. (7) and (8)]. For very large matter potentials, on the other hand, the mixing between ν_{iS} and ν_{iA} decreases, reaching the limit $\lambda_{iS} = A/2 + m^2_i/2$ and $\lambda_{iA} = -A/2 + m^2_i/2$.

In the scenario where the matter potential is constant along the neutrino evolution path, we can find the neutrino oscillation probability using the mixing angles and

[4] For simplicity, we assume that the CνB matter effect is flavor-universal. This is certainly valid if the CνB contains neutrinos of all flavor with equal number densities and if they interact only via weak interactions. Decaying neutrinos [87, 88] or the presence of flavor-nonuniversal nonstandard interactions [89] would need special treatment.

the eigenvalues from above. Considering the $\nu_\alpha \to \nu_\beta$ oscillation probability between the active states, we get

$$P_{\alpha\beta} = \sum_j \left| U_{\alpha j} U^\dagger_{\beta j} \left[\cos^2\widetilde{\theta}_j \exp\left(\frac{-i\lambda_{jS}L}{2E_\nu}\right) + \sin^2\widetilde{\theta}_j \exp\left(\frac{-i\lambda_{jA}L}{2E_\nu}\right)\right]\right|^2 , \tag{14}$$

where L is the propagation length. The oscillation length induced by the active-active mass splitting Δm^2_{j1}, which is equal to $\Delta m^2_{\rm sol} \simeq 7.4\times10^{-5}$ eV^2 for $j=2$ and $\Delta m^2_{\rm atm} \simeq 2.5\times10^{-3}$ eV^2 for $j=3$ [83], is much shorter than the distance traveled by astrophysical neutrinos [cf. Eq. (2)] and is impossible to be resolved by the present detectors. Therefore, we average over it, thus obtaining

$$P_{\alpha\beta} = \sum_j |U_{\alpha j}|^2 |U_{\beta j}|^2 \left[\cos^4\widetilde{\theta}_j + \sin^4\widetilde{\theta}_j + 2\cos^2\widetilde{\theta}_j \sin^2\widetilde{\theta}_j \cos\left(\frac{\delta\widetilde{m}^2_j L}{4E_\nu}\right)\right] , \tag{15}$$

where the effective mass-squared splitting in the presence of matter effect is given by

$$\delta\widetilde{m}^2_j = \sqrt{A^2 - 2A\delta m^2_j\cos(2\theta_j) + (\delta m^2_j)^2} \simeq \sqrt{(\delta m^2_j)^2 + A^2} , \tag{16}$$

which reduces to the vacuum mass-squared splitting δm^2_i when $A \ll \delta m^2_j$, as expected. The effective active-sterile oscillation length scale in the presence of matter is

$$L_{\rm osc} = \frac{4\pi E_\nu}{\delta\widetilde{m}^2_j} , \tag{17}$$

which now explicitly depends on the matter potential via Eq. (16). It reduces to the vacuum case [cf. Eq. (2) with $\Delta m^2 \to \delta m^2$] when $A \ll \delta m^2_i$.

One might wonder whether the interactions of the high-energy neutrinos with the free electrons in the intergalactic medium (IGM) could also induce additional matter effect for the small δm^2 values under consideration. The mean IGM electronic density is $n_e \sim 10^{-7}$ cm^{-3} [90], which corresponds to a matter potential $V_e = \sqrt{2}G_F n_e \sim 10^{-44}$ eV. Even for a PeV-energy neutrino (the highest energy observed by IceCube), such a tiny matter potential will only be relevant if $\delta m^2 \sim 10^{-29}$ eV^2. However, in this case, the corresponding effective oscillation length is way beyond the size of the observable Universe, as we will see later. Therefore, we can safely neglect the IGM matter effect and only consider the CνB matter effect.

IV. PSEUDO-DIRAC NEUTRINOS IN EXPANDING UNIVERSE

As the universe expands, the neutrino density from the CνB reduces. Considering that the neutrino density scales with the redshift as $n_\nu = n_{\nu,0}(1+z)^3$, we have a matter potential that changes with redshift, or in other words, with time.

To estimate whether the neutrino evolution in an expanding universe is adiabatic or not, we have to compare the inverse oscillation length $(\delta\widetilde{m}^2/2E_\nu)$ with the transition between the massive states that is proportional to the variation of the effective mixing angle in matter $(d\widetilde{\theta}/dx)$. Defining the adiabaticity parameter (γ) as the ratio between these two quantities [80], we have

$$\gamma = \frac{\delta\widetilde{m}^2}{2E_\nu}\frac{1}{|d\widetilde{\theta}/dx|} = \frac{2}{3}\frac{\delta\widetilde{m}^2(1+z)}{E_\nu \sin 4\widetilde{\theta}(dz/dx)} , \tag{18}$$

where dz/dx is given by the expansion rate of the universe. For $\delta m^2 \geq 10^{-17}$eV^2 and $E_\nu < 1$ PeV, we have $\gamma > 1$, which indicates that the evolution is adiabatic. In this adiabatic regime, the $\nu_\alpha \to \nu_\beta$ oscillation probability is given by

$$P_{\alpha\beta} = \sum_j |U_{\alpha j}|^2 |U_{\beta j}|^2 \left[\cos^2\widetilde{\theta}^i_j \cos^2\widetilde{\theta}^f_j + \sin^2\widetilde{\theta}^i_j \sin^2\widetilde{\theta}^f_j + \frac{1}{2}\sin 2\widetilde{\theta}^i_j \sin 2\widetilde{\theta}^f_j \cos\left(\int dx \frac{\delta\widetilde{m}^2_j}{4E_\nu}\right)\right] , \tag{19}$$

where $\widetilde{\theta}^i$ and $\widetilde{\theta}^f$ correspond to the effective mixing angles [cf. Eq. (10)] when the neutrinos were created and today, respectively. When the matter effect is small, $\widetilde{\theta}^i_j \simeq \widetilde{\theta}^f_j \simeq \widetilde{\theta}_j$ and $\delta\widetilde{m}^2_j$ can be taken out of the integral. In this case, Eq. (19) simply reduces to Eq. (15). In the parameter regime where the adiabaticity condition is not satisfied, we cannot express the oscillation probability analytically as in Eq. (19). In such cases, we compute the oscillation probability purely numerically from the solution of the evolution equation, i.e. $\langle\nu_\beta|\nu_\alpha\rangle(t) = \exp[-i\int_0^t dt' H(t')]$.

Note that in Eq. (19), the effective oscillation length, as well as $\delta\widetilde{m}^2_j$, is now a function of the redshift. In particular, for the active-sterile oscillations to take effect, the oscillation length $L_{\rm osc}$ must be comparable to or smaller than the effective source distance, given by [16]

$$L_{\rm eff} = \int_{z_{\rm min}}^{z_{\rm max}} \frac{c\,dz}{H(z)(1+z)^2} , \tag{20}$$

where the Hubble parameter is

$$H(z) = H_0\sqrt{\Omega_{\rm m}(1+z)^3 + \Omega_\Lambda + (1-\Omega_{\rm m}-\Omega_\Lambda)(1+z)^2} , \tag{21}$$

where $\Omega_{\rm m}$ and Ω_Λ are the fractions of matter (both visible and dark) and dark energy content in the Universe, respectively. We use the best-fit values from Planck data: $\Omega_{\rm m} = 0.315$, $\Omega_\Lambda = 0.685$ and $H_0 = 67.4$ km $\cdot$ s^{-1} $\cdot$ Mpc^{-1} [91]. Because of this choice of the unit for H_0, we have shown the speed of light c explicitly in Eq. (20) to make it dimensionally correct. As for the maximum redshift value, we will take $z_{\rm max} = 5$, beyond which the

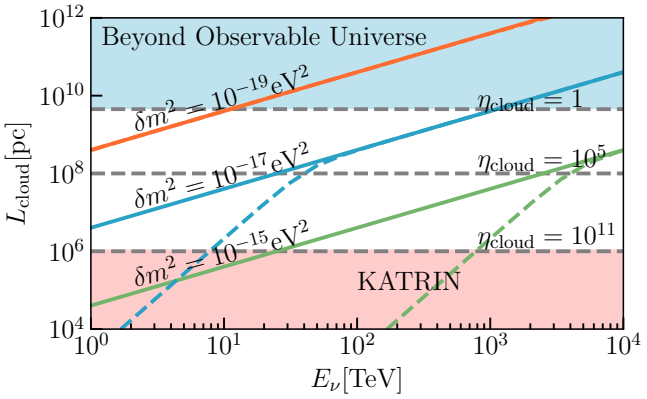

FIG. 1. The active-sterile mass splittings in vacuum (δm^2, solid) and including CνB matter effect ($\delta\widetilde{m}^2$, dashed) as a function of the neutrino energy. The vertical axis shows the maximum size of the overdense CνB cluster for a given value of overdensity $\eta_{\rm cloud}$, demanding that the total number of relic neutrinos in the Universe is constant. The red-shaded region at the bottom corresponds to the KATRIN exclusion limit on $\eta < 1.1\times10^{11}$ at 95% CL [95]. The blue-shaded region at the top corresponds to oscillation lengths beyond the observable Universe.

star formation rate decreases rapidly [92, 93], and we do not expect any astrophysical sources of high-energy neutrinos to exist beyond this redshift. Similarly, for the minimum redshift, we take $z_{\rm min} = 10^{-7}$, corresponding to the galactic center. Since the galactic contribution to the high-energy neutrino flux at IceCube is subdominant [94], taking even smaller values of $z_{\rm min}$ will not significantly affect our results.

V. INCLUDING CνB OVERDENSITY

The values of δm^2 that are sensitive to the CνB matter effect very much depend on the incoming energy of the high-energy neutrinos. This is illustrated in Fig. 1 by the solid lines for three benchmark values of δm^2. The corresponding dashed lines show the fixed $\delta\widetilde{m}^2$ values. The deviation of the dashed lines from the solid lines, therefore, represent the size of the matter effect. As we will see below, the CνB matter effect on the oscillation probabilities turns out to be negligible for the ΛCDM value of the CνB number density [cf. Eq. (11)], especially for the δm^2 values required for adiabatic evolution. Therefore, we allow for the possibility that there might be a local overdensity of CνB, parameterized by the ratio $\eta = n_\nu/n_{\nu,0}(1+z)^3$. The current experimental limit on η is rather loose, only at the level of 10^{11} from KATRIN [95], as shown by the red-shaded region in Fig. 1. See Refs. [96–102] for other local and global constraints on η, as well as future prospects. We assume a local overdensity around the Earth so that the matter effect is isotropic. Theoretically, while gravitational clustering alone can only give an $\mathcal{O}(1)$ enhancement [103–107], possible nonstandard neutrino interactions could in principle give $\eta \gg 1$. For instance, in a model with Yukawa interactions mediated by an ultralight scalar, neutrinos can form stable clusters with $\eta_{\rm max} \sim 10^7$ [108]. Without resorting to any particular new physics model, we just show a few benchmark values of η in Fig. 1 to illustrate our point. Note that for smaller η values, the δm^2 and $\delta\widetilde{m}^2$ contours are identical, i.e. the matter effect is negligible. However, for $\eta \gtrsim 10^5$, we start to see the deviation of $\delta\widetilde{m}$ from δm^2, which implies that the matter effect is non-negligible.

An important thing to keep in mind is that, for a fixed number of total relic neutrinos in the Universe, $\eta > 1$ would imply that there is a maximum size for the overdense cluster, $L_{\rm cloud} = (c/H_0)\eta^{-1/3}$ assuming a spherical cluster. This is to ensure that the relic neutrinos do not overclose the Universe. For instance, as shown in Fig. 1, $\eta = 1$ corresponds to $L_{\rm cloud} = c/H_0 \simeq 4.5$ Gpc, which is roughly the size of the observable Universe, whereas $\eta = 10^5$ corresponds to $L_{\rm cloud} \simeq 96$ Mpc, and $\eta = 10^{11}$ corresponds to $L_{\rm cloud} \simeq 0.96$ Mpc. Therefore, for the matter effect to be relevant, we must have the effective oscillation length $L_{\rm osc}$ [cf. Eq. (17)] comparable to or smaller than $L_{\rm cloud}$.

This in turn dictates the minimum value of δm^2 (for a given E_ν), or the maximum value of E_ν (for a given δm^2), at which the matter effect starts becoming important. For example, for $\delta m^2 = 10^{-19}$ eV^2, the matter effect is not important in the entire energy range shown in Fig. 1, whereas for $\delta m^2 = 10^{-17}$ eV^2, it starts becoming important for $E_\nu < 70$ TeV, and for $\delta m^2 = 10^{-15}$ eV^2, it is important for $E_\nu < 70$ PeV, i.e. almost in the entire IceCube energy range of interest. However, this does not necessarily mean that IceCube has better sensitivity for higher δm^2 values, as this will depend on the actual oscillation probabilities, which we will discuss in Section VI.

For $\eta > 1$, or a finite $L_{\rm cloud} < c/H_0$, we have to consider the case where the neutrinos were emitted from the distant source at an early redshift ($z_i \le z_{\rm max}$) and, after traveling through vacuum for some distance, encounter the CνB overdensity cloud at a redshift $z_c < z_i$ that creates a matter potential for them. In this case, the oscillation probability contains two parts: (i) vacuum probability from redshift z_c to z_i, and (ii) matter probability from redshift $z_{\rm min}$ and z_c. Thus, Eq. (19) is modified to

$$P_{\alpha\beta} = \frac{1}{2}\sum_j |U_{\alpha j}|^2|U_{\beta j}|^2\left[1+\cos 2\widetilde{\theta}_j^i\cos 2\widetilde{\theta}_j^f\cos\left(\frac{\delta m_j^2 L_{\rm eff}}{4E_\nu}\right)+\sin 2\widetilde{\theta}_j^i\sin 2\widetilde{\theta}_j^f\cos\left(\int dx\frac{\delta\widetilde{m}_j^2}{4E_\nu}+\frac{\delta m_j^2 L_{\rm eff}}{4E_\nu}\right)\right]. \quad (22)$$

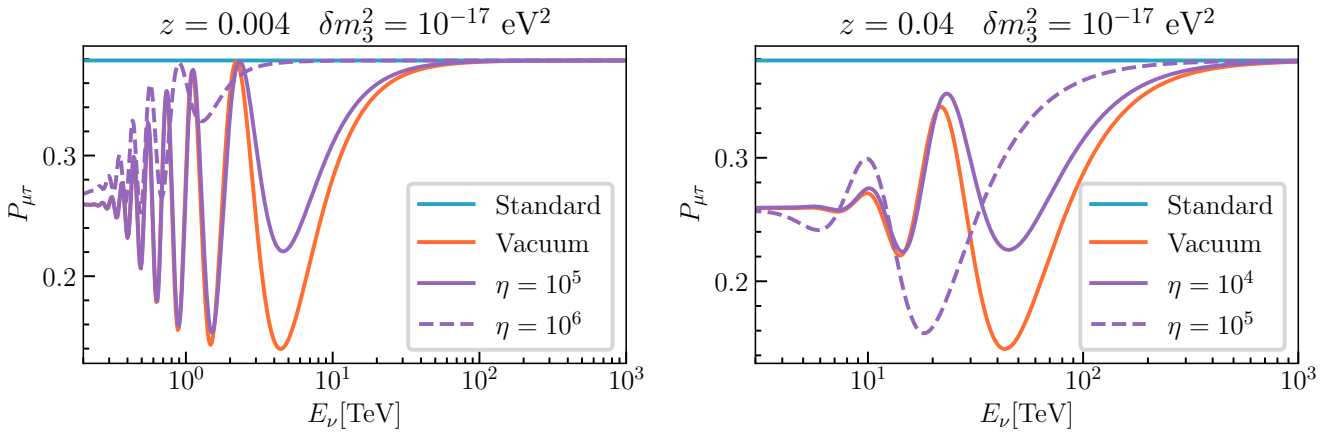

FIG. 2. $\mu \to \tau$ oscillation probability as a function of neutrino energy for the pseudo-Dirac case in vacuum only (orange) and including the CνB matter effect (purple) with two benchmark values of η (solid and dashed). Here we have fixed $\delta m_3^2 = 10^{-17}$ eV^2 and $z = 0.004$ (0.04) in the left (right) panel. The fast oscillations at low energies are averaged out. The averaged oscillation probability in the standard 3-neutrino case (blue) is also shown for comparison.

Notice that in this case, $\widetilde{\theta}^i$ and $\widetilde{\theta}^f$ correspond to the effective mixing angles when the neutrinos arrive to the CνB cloud and today, respectively. Also, $L_{\rm eff}$ is given by Eq. (20) but with the lower limit of integration replaced by z_c, which is the redshift distance equivalent of $L_{\rm cloud}$. Basically, in vacuum, we can take δm^2 out of the redshift integral, whereas in matter, we have to keep $\delta \widetilde{m}^2$ inside the integral, since it also depends on the redshift. For $\eta \lesssim 10^4$, when the matter effect is negligible, the last two contributions inside the parenthesis can be combined into one that exactly becomes equal to $\delta m_j^2 L_{\rm eff}/4E_\nu$ as in the second term, and Eq. (22) simply reduces to the vacuum oscillation result [cf. Eq. (19) with tildes removed].

VI. RESULTS

To understand the energy dependence of the oscillation probabilities in the presence of matter effect, we plot the $\nu_\mu \to \nu_\tau$ oscillation probabilities[5] for the standard and pseudo-Dirac cases (with and without matter effect) in Fig. 2. Here we have fixed the active-sterile mass splitting for just one pair: $\delta m_3^2 = 10^{-17}$ eV^2, while keeping $\delta m_1^2 = \delta m_2^2 = 0$. In the left panel, we have fixed the source redshift distance at $z = 0.004$, which is roughly the distance to NGC 1068, the most significant point source identified by IceCube [45]. The vacuum oscillation probability for the pseudo-Dirac case is noticeably different from the standard case for $E_\nu \lesssim 50$ TeV. At higher energies, the effective oscillation length exceeds the source distance, and therefore, the vacuum oscillation probability approaches the standard case. On the other hand, at low energies, the fast oscillations are averaged out to a constant value (but different from the standard case). Now including the matter effect further modifies the oscillation probability, as it tends to suppress the oscillation amplitude, as compared to the vacuum case. But this effect is observable only for $\eta \gg 1$, because the source is relatively nearby, so we need a large η to be able to make a significant contribution to the third term in Eq. (22). Here we have chosen two benchmark values of $\eta = 10^5$ and $\eta = 10^6$. As we increase the size of the matter effect by cranking up η, the oscillation extrema are also shifted to lower energies.

In the right panel of Fig. 2, we keep the same $\delta m_3^2 = 10^{-17}$ eV^2, but increase the source distance to $z = 0.04$. In this case, the oscillations are shifted to higher energies, and the pseudo-Dirac oscillations are noticeably different from the standard one for $E_\nu \lesssim 500$ TeV. Also, since the source is further away, a slightly smaller value of $\eta = 10^4$ is now sufficient to induce a noticeable matter effect. As in the left panel, increasing η shifts the oscillation extrema to lower energies, before they approach the fast oscillations. Since getting very large η values is theoretically challenging, we will fix a benchmark value of $\eta = 10^4$ and $z = 0.04$ for the flavor triangle analysis below.

For a given source distance, if we increase the δm^2 value, the oscillations will also be shifted to higher energies. Since the astrophysical neutrino flux is expected to have a power-law behavior [109], going to higher energy means having smaller flux, and hence, less statistics. It turns out that IceCube will eventually lose sensitivity for $\delta m^2 \gtrsim 10^{-16}$ eV^2 [16]. Therefore, we use $\delta m^2 = 10^{-17}$ eV^2 as our benchmark value.

In Fig. 3, we have plotted the same $\nu_\mu \to \nu_\tau$ probabilities for the standard and pseudo-Dirac (vacuum and matter) cases as a function of energy, but here we have

[5] Similar behavior is observed for other flavors, and therefore, we do not show all of them here.

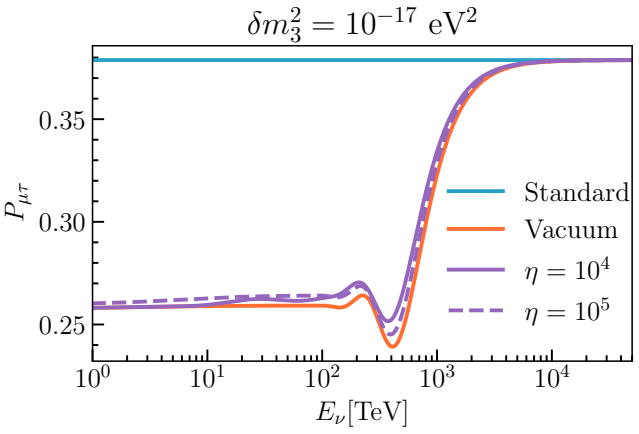

FIG. 3. Same as in Fig. 2, but here we have averaged over the distance traveled by the neutrinos and have assumed a flat distribution of sources up to $z = 5$.

averaged over the the distances up to redshift $z_{\rm max} = 5$, assuming a flat distribution of sources. The first dip in the probability at the highest energy is due to contributions from sources at $z = 5$. We note that increasing η (or decreasing the cloud size) makes this dip closer to the vacuum case because the neutrinos mostly travel in vacuum; therefore, going to an arbitrarily high overdensity is actually not helpful for disentangling the matter effect. As we go to lower energies, the sources at smaller redshifts cause multiple oscillations, which eventually average out and approach the vacuum result, as also noted in Fig. 2. On the other hand, both vacuum and matter oscillations approach the standard result at energies beyond 5 PeV, since the effective oscillation length for the chosen mass splitting goes beyond $z = 5$.

Note that we have only shown the probability results for neutrinos. For anti-neutrinos, the matter potential changes sign, and the results are similar, unless there is a large asymmetry between neutrinos and antineutrinos in the CνB. The current cosmological constraints on this asymmetry, parameterized in terms of the degeneracy parameters $\xi_\alpha \equiv \mu_\alpha/T$ (where μ_α's are the chemical potentials) by

$$\eta_{\nu_\alpha} \equiv \frac{n_{\nu_\alpha} - n_{\bar\nu_\alpha}}{n_\gamma} \simeq 0.25\xi_{\nu_\alpha}\left(1 + \frac{\xi_{\nu_\alpha}^2}{\pi^2}\right), \qquad (23)$$

allow for η_ν as large as 10^{-2} [110]. In fact, the recent ^{4}He measurements from extremely metal-poor galaxies has a mild preference for a non-zero electron neutrino chemical potential: $\xi_{\nu_e} = 0.043 \pm 0.015$ [111, 112]. However, we have checked that to get an observable difference in the matter effect for neutrinos versus antineutrinos, we need $\eta_{\nu_\alpha} \gtrsim \mathcal{O}(1)$, which is highly unlikely given the current constraints.

After calculating the effect of pseudo-Dirac neutrino oscillations on the probabilities, we are now in a position to compare the final flavor ratio results for the standard and pseudo-Dirac case with and without matter effect. This is shown in Fig. 4. Note that it is important to compare only the normalized flavor ratios, because the total flux of active neutrinos in the pseudo-Dirac case may not be conserved due to active-sterile oscillations; therefore, $\sum_\beta f_{\beta,\oplus}$ calculated from Eq. (4) is not necessarily guaranteed to be unity for the pseudo-Dirac case, unlike in the standard case. Here we take a standard pion decay source:

$$\pi^\pm \to \mu^\pm + \overset{(-)}{\nu}_\mu \to e^\pm + \overset{(-)}{\nu}_e + \nu_\mu + \bar\nu_\mu\,, \qquad (24)$$

with an initial flavor composition of $(1/3 : 2/3 : 0)$. With the best-fit values for the oscillation parameters taken from `NuFit` [83] and assuming a normal mass ordering, the standard 3-neutrino vacuum oscillation paradigm predicts a final flavor ratio of $(0.33 : 0.35 : 0.32)$, as shown by the blue dot. On the other hand, for our benchmark pseudo-Dirac case with $\delta m_3^2 = 10^{-17}$ eV^2, just considering vacuum oscillations from a source at redshift $z = 0.04$ gives us $(0.46 : 0.30 : 0.24)$ at $E_\nu = 1$ TeV and $(0.42 : 0.32 : 0.26)$ at $E_\nu = 40$ TeV, as shown by the orange dots in the two panels. Note the mild energy-dependence of the best-fit value here. This was also noted in Ref. [39].

Including the CνB matter effect for an overdensity of $\eta = 10^4$ makes the energy-dependent effects more prominent in the oscillation probabilities (see Figs. 2 and 3). In the left panel, we show the result for $E_\nu = 1$ TeV, where the matter effect gives a best-fit flavor ratio of $(0.44 : 0.31 : 0.25)$, while in the right panel with $E_\nu = 40$ TeV, it gives $(0.36 : 0.34 : 0.30)$. Thus, as we go from lower to higher energies, the best-fit point moves from the vacuum case to the standard case, as can be clearly seen from the inset plots. The energy window of TeV-PeV is optimal for this effect to be observable. For very high energies, the neutrino flux goes down rapidly and the event statistics will be low. On the other hand, for energies smaller than a few TeV, the atmospheric background will be overwhelming. Moreover, the tau neutrinos are not detectable at IceCube for low energies; the lowest-energy tau event observed so far is at 20 TeV [113].

In Fig. 4, the current 68% and 90% CL IceCube limits [114] are shown by the black contours.[6] The future prospects for flavor triangle measurements are bright [116], with the observation of high-energy neutrinos by several next-generation neutrino telescopes, such as IceCube-Gen 2 [54], KM3NeT [51], Baikal-GVD [55], P-ONE [56], TRIDENT [57], TAMBO [58], Trinity [59] and RET [60]. The possibility of a joint analysis of the combined data from multiple experiments sensitive to different neutrino flavors (e.g., cascade and track data from

[6] Preliminary tighter constraints are reported in Ref. [115] by adding more years of data and updated ice properties on the HESE sample, but we show the officially published results from Ref. [114].

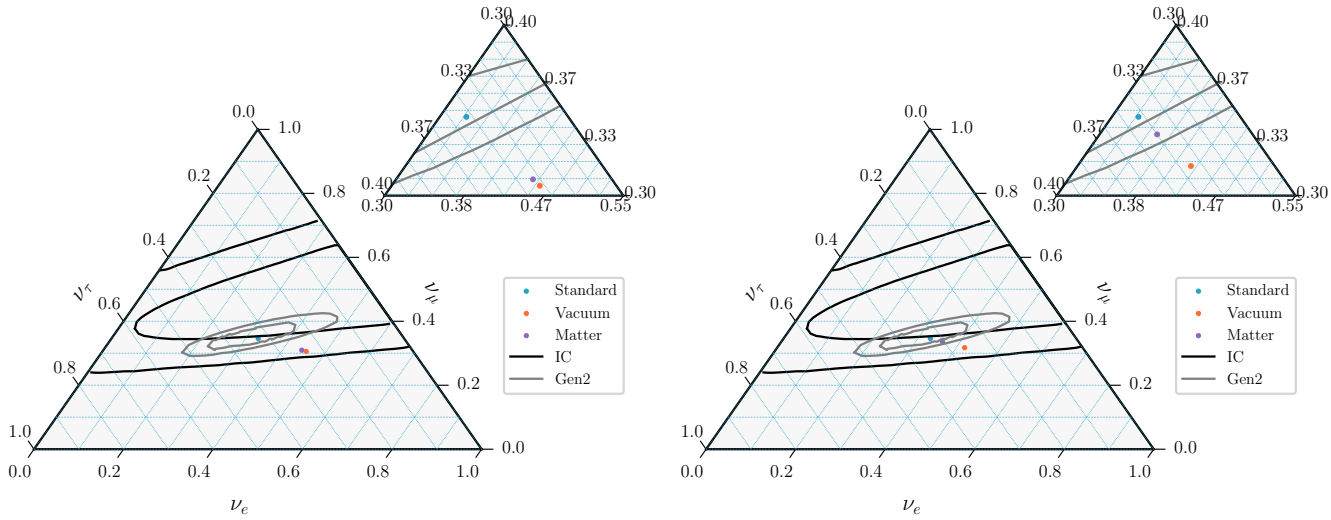

FIG. 4. CνB matter effect on the best-fit point in the flavor triangle for $E_\nu = 1$ TeV (left) and 40 TeV (right). With increasing energy, the best-fit point for the pseudo-Dirac case in the presence of matter effect (purple) moves from the vacuum case (orange) toward the standard 3-neutrino case (light blue). Here we have fixed $\delta m_3^2 = 10^{-17}$ eV^2, $z = 0.04$ and have considered the standard pion source with initial flavor ratio $(1/3 : 2/3 : 0)$. For the matter case, we have fixed $\eta = 10^4$.

IceCube-Gen 2, combined with the tau-neutrino data from TAMBO) could significantly improve the precision on the flavor triangle data. For illustration, we show the IceCube-Gen 2 projections [117] by the grey contours. It is clear that while the current IceCube constraint is not enough to probe the CνB matter effect, the IceCube-Gen 2 will be able to do so. In fact, it can clearly distinguish the energy-dependent matter effect from the vacuum oscillations, which will provide a new way to probe the CνB overdensity, on top of probing the pseudo-Dirac hypothesis.

In Fig. 5, we fix the energy at 40 TeV, but generalize our analysis to different initial flavor compositions, as mentioned in Section I, namely, (i) standard pion decay (top left panel), (ii) muon-suppressed pion decay (top right panel), (iii) neutron decay (bottom left panel), and (iv) general case (bottom right panel). We also include the variation of the mixing angles in their 68% CL allowed range from `NuFit` [83], which results in a spread of the points for each case. Our use of the reduced uncertainties (68% CL) is in anticipation of the precision measurements of the oscillation parameters at next-generation neutrino oscillation experiments, such as JUNO [118], DUNE [119], and Hyper-K [120], before the next-generation neutrino telescopes start collecting data. We find that with improved precision on the oscillation parameters, it is possible to completely separate the standard case from the pseudo-Dirac case for a known initial flavor composition at a given energy. The energy-dependent effect shown in Fig. 4 will make this distinction even easier. We also notice that the separation from the standard case on the flavor triangle is different, depending on the initial flavor composition and on which δm_i^2 is nonzero. This information will provide a unique way to probe the individual active-sterile mass splittings in the pseudo-Dirac scenario.

In Fig. 6, we further generalize our analysis to include two active-sterile mass splittings nonzero (but equal). Even in this case, the distinction between the standard and pseudo-Dirac cases, as well as between the different δm_i^2 pairs, can be made for a known initial flavor ratio. Of course, if the initial flavor composition is not known precisely, it becomes more difficult to distinguish the pseudo-Dirac case, as shown in the lower right panels of Figs. 5 and 6.

Finally, when we have all three mass splittings nonzero and equal, their effect on the flavor ratio cancels out and there is no longer any difference with the standard case.

VII. CONCLUSIONS

The flavor ratio measurements of the high-energy astrophysical neutrinos at neutrino telescopes provide crucial information on the source properties. We have shown that the flavor ratio predictions are altered from the standard 3-neutrino paradigm if neutrinos are pseudo-Dirac particles with tiny active-sterile mass splittings. In particular, we find for the first time that the CνB matter effect induces a novel energy-dependent flavor effect, which is robust against energy reconstruction, and hence, can be distinguished from other sources of energy dependence. We therefore advocate making energy-dependent flavor triangle measurements at neutrino telescopes. Energy-dependent flavor composition measurements were also advocated recently in Ref. [77] for a different physics reason, i.e. to establish the transition from neutrino production via the full pion decay chain at low

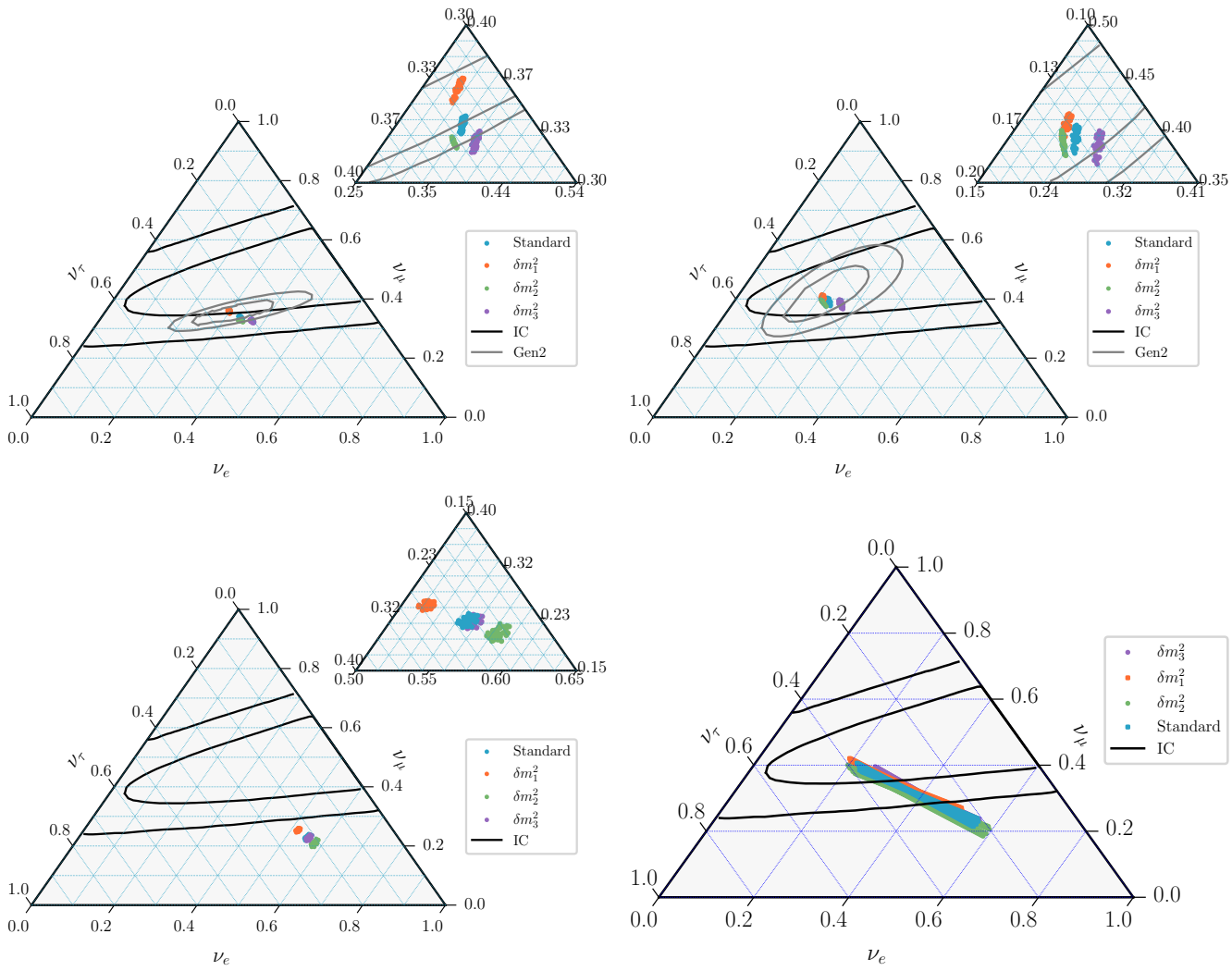

FIG. 5. Ternary plots for the neutrino flavor composition on Earth for four different benchmark source flavor compositions (i) (1/3:2/3:0), (ii) (0:1:0), (iii) (1:0:0), (iv) $(x : 1-x : 0)$. Here we compare the standard 3-neutrino oscillation paradigm with the pseudo-Dirac case with one active-sterile mass splitting nonzero. We have fixed the distance at $z = 0.04$ and the neutrino energy at 40 TeV. For the matter case, we have fixed $\eta = 10^4$.

energies to muon-damped pion decay at high energies. This is challenging today, but may be feasible in the future. Moreover, the matter effect strongly depends on the local CνB overdensity, and therefore, a precise determination of the flavor composition at future neutrino telescopes can in principle provide an alternative probe of the CνB overdensity.

ACKNOWLEDGMENTS

This work of BD was partly supported by the U.S. Department of Energy under grant No. DE-SC 0017987. PM is supported by Fermi Research Alliance, LLC under Contract No. DE-AC02-07CH11359 with the U.S. Department of Energy, Office of Science, Office of High Energy Physics. IMS is supported by STFC grant ST/T001011/1. BD and PM thank the organizers of the Mitchell Conference 2023, where this work was initiated. We also acknowledge the Center for Theoretical Underground Physics and Related Areas (CETUP*) and the Institute for Underground Science at SURF for hospitality and for providing a stimulating environment, where a part of this work was done.

Note Added: While we were completing this work, Ref. [121] appeared, where the authors also discuss the effect of pseudo-Dirac neutrinos on the flavor triangle. But they have not included the CνB matter effect.

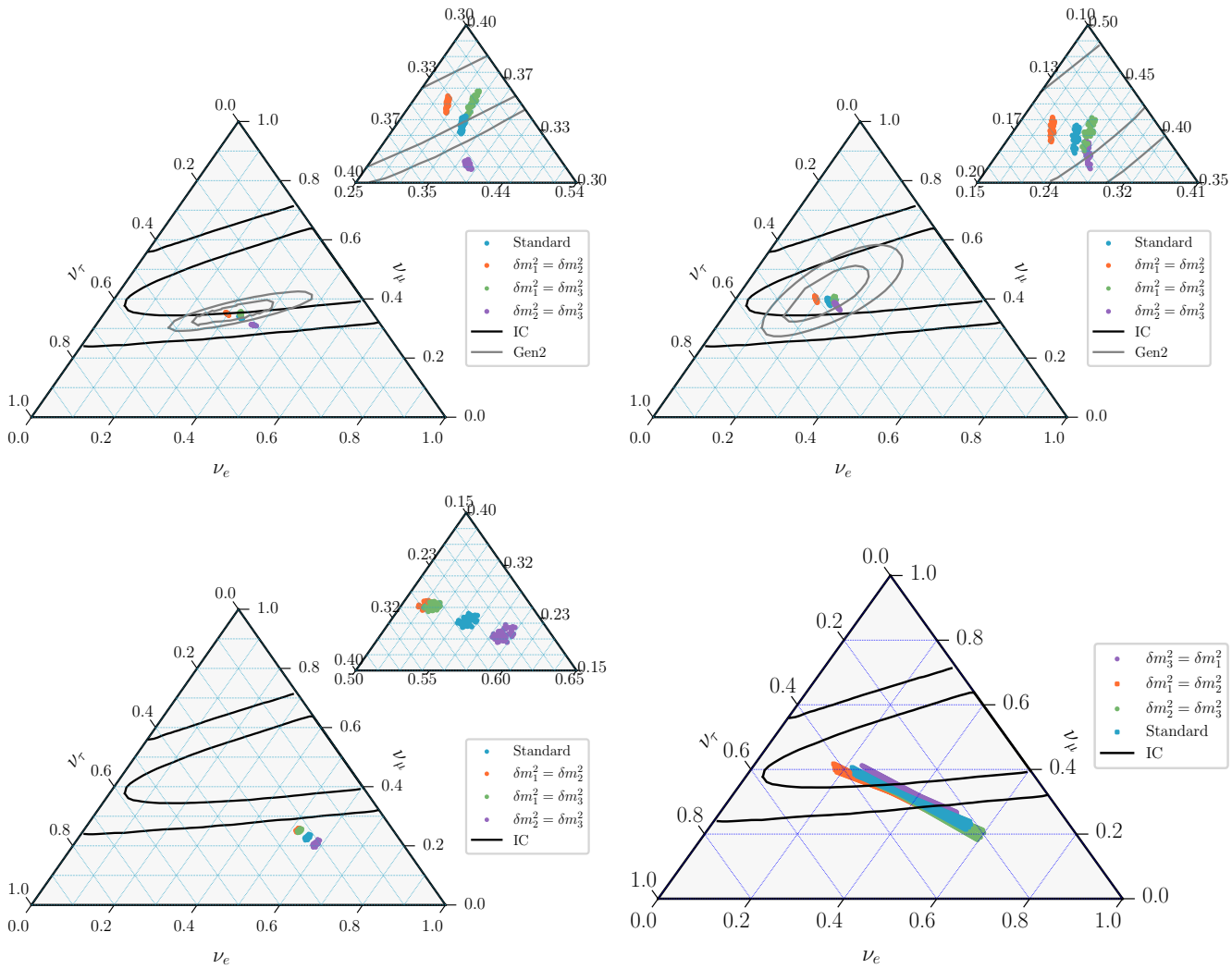

FIG. 6. Same as Fig. 4, but with two active-sterile mass splittings nonzero.

[1] L. Wolfenstein, "Different Varieties of Massive Dirac Neutrinos," *Nucl. Phys. B* **186** (1981) 147–152.

[2] S. T. Petcov, "On Pseudodirac Neutrinos, Neutrino Oscillations and Neutrinoless Double beta Decay," *Phys. Lett. B* **110** (1982) 245–249.

[3] J. W. F. Valle and M. Singer, "Lepton Number Violation With Quasi Dirac Neutrinos," *Phys. Rev. D* **28** (1983) 540.

[4] M. Doi, M. Kenmoku, T. Kotani, H. Nishiura, and E. Takasugi, "PSEUDODIRAC NEUTRINO," *Prog. Theor. Phys.* **70** (1983) 1331.

[5] M. Kobayashi and C. S. Lim, "Pseudo Dirac scenario for neutrino oscillations," *Phys. Rev. D* **64** (2001) 013003, arXiv:hep-ph/0012266.

[6] D. Chang and O. C. W. Kong, "Pseudo-Dirac neutrinos," *Phys. Lett. B* **477** (2000) 416–423, arXiv:hep-ph/9912268.

[7] Y. Nir, "PseudoDirac solar neutrinos," *JHEP* **06** (2000) 039, arXiv:hep-ph/0002168.

[8] A. S. Joshipura and S. D. Rindani, "Phenomenology of pseudoDirac neutrinos," *Phys. Lett. B* **494** (2000) 114–123, arXiv:hep-ph/0007334.

[9] M. Lindner, T. Ohlsson, and G. Seidl, "Seesaw mechanisms for Dirac and Majorana neutrino masses," *Phys. Rev. D* **65** (2002) 053014, arXiv:hep-ph/0109264.

[10] K. R. S. Balaji, A. Kalliomaki, and J. Maalampi, "Revisiting pseudoDirac neutrinos," *Phys. Lett. B* **524** (2002) 153–160, arXiv:hep-ph/0110314.

[11] G. J. Stephenson, Jr., J. T. Goldman, B. H. J. McKellar, and M. Garbutt, "Large mixing from small: PseudoDirac neutrinos and the singular seesaw," *Int. J. Mod. Phys. A* **20** (2005) 6373–6390, arXiv:hep-ph/0404015.

[12] K. L. McDonald and B. H. J. McKellar, "The Type-II Singular See-Saw Mechanism," *Int. J. Mod. Phys. A* **22** (2007) 2211–2222, arXiv:hep-ph/0401073.

[13] Y. H. Ahn, S. K. Kang, and C. S. Kim, "A Model for Pseudo-Dirac Neutrinos: Leptogenesis and Ultra-High Energy Neutrinos," *JHEP* **10** (2016) 092, arXiv:1602.05276 [hep-ph].

[14] A. S. Joshipura, S. Mohanty, and S. Pakvasa, "Pseudo-Dirac neutrinos via a mirror world and depletion of ultrahigh energy neutrinos," *Phys. Rev. D* **89** no. 3, (2014) 033003, arXiv:1307.5712 [hep-ph].

[15] K. S. Babu, X.-G. He, M. Su, and A. Thapa, "Naturally light Dirac and pseudo-Dirac neutrinos from left-right symmetry," *JHEP* **08** (2022) 140, arXiv:2205.09127 [hep-ph].

[16] K. Carloni, I. Martínez-Soler, C. A. Arguelles, K. S. Babu, and P. S. B. Dev, "Probing pseudo-Dirac neutrinos with astrophysical sources at IceCube," *Phys. Rev. D* **109** (2024) L051702, arXiv:2212.00737 [astro-ph.HE].

[17] H. Ooguri and C. Vafa, "Non-supersymmetric AdS and the Swampland," *Adv. Theor. Math. Phys.* **21** (2017) 1787–1801, arXiv:1610.01533 [hep-th].

[18] L. E. Ibanez, V. Martin-Lozano, and I. Valenzuela, "Constraining Neutrino Masses, the Cosmological Constant and BSM Physics from the Weak Gravity Conjecture," *JHEP* **11** (2017) 066, arXiv:1706.05392 [hep-th].

[19] E. Gonzalo, L. E. Ibáñez, and I. Valenzuela, "Swampland constraints on neutrino masses," *JHEP* **02** (2022) 088, arXiv:2109.10961 [hep-th].

[20] G. F. Casas, L. E. Ibáñez, and F. Marchesano, "On small Dirac Neutrino Masses in String Theory," arXiv:2406.14609 [hep-th].

[21] C. S. Fong, T. Gregoire, and A. Tonero, "Testing quasi-Dirac leptogenesis through neutrino oscillations," *Phys. Lett. B* **816** (2021) 136175, arXiv:2007.09158 [hep-ph].

[22] M. Chianese, P. Di Bari, K. Farrag, and R. Samanta, "Probing relic neutrino radiative decays with 21 cm cosmology," *Phys. Lett. B* **790** (2019) 64–70, arXiv:1805.11717 [hep-ph].

[23] P. S. B. Dev, P. Di Bari, I. Martínez-Soler, and R. Roshan, "Relic neutrino decay solution to the excess radio background," *JCAP* **04** (2024) 046, arXiv:2312.03082 [hep-ph].

[24] C. Giunti, C. W. Kim, and U. W. Lee, "Oscillations of pseudoDirac neutrinos and the solar neutrino problem," *Phys. Rev. D* **46** (1992) 3034–3039, arXiv:hep-ph/9205214.

[25] M. Cirelli, G. Marandella, A. Strumia, and F. Vissani, "Probing oscillations into sterile neutrinos with cosmology, astrophysics and experiments," *Nucl. Phys. B* **708** (2005) 215–267, arXiv:hep-ph/0403158.

[26] A. de Gouvea, W.-C. Huang, and J. Jenkins, "Pseudo-Dirac Neutrinos in the New Standard Model," *Phys. Rev. D* **80** (2009) 073007, arXiv:0906.1611 [hep-ph].

[27] G. Anamiati, R. M. Fonseca, and M. Hirsch, "Quasi Dirac neutrino oscillations," *Phys. Rev. D* **97** no. 9, (2018) 095008, arXiv:1710.06249 [hep-ph].

[28] A. de Gouvêa, E. McGinness, I. Martinez-Soler, and Y. F. Perez-Gonzalez, "pp solar neutrinos at DARWIN," *Phys. Rev. D* **106** no. 9, (2022) 096017, arXiv:2111.02421 [hep-ph].

[29] S. Ansarifard and Y. Farzan, "Revisiting pseudo-Dirac neutrino scenario after recent solar neutrino data," (11, 2022) , arXiv:2211.09105 [hep-ph].

[30] J. Franklin, Y. F. Perez-Gonzalez, and J. Turner, "JUNO as a Probe of the Pseudo-Dirac Nature using Solar Neutrinos," arXiv:2304.05418 [hep-ph].

[31] A. De Gouvêa, I. Martinez-Soler, Y. F. Perez-Gonzalez, and M. Sen, "Fundamental physics with the diffuse supernova background neutrinos," *Phys. Rev. D* **102** (2020) 123012, arXiv:2007.13748 [hep-ph].

[32] I. Martinez-Soler, Y. F. Perez-Gonzalez, and M. Sen, "Signs of pseudo-Dirac neutrinos in SN1987A data," *Phys. Rev. D* **105** no. 9, (2022) 095019, arXiv:2105.12736 [hep-ph].

[33] R. M. Crocker, F. Melia, and R. R. Volkas, "Oscillating Neutrinos from the Galactic Center," *Astrophys. J. Suppl. Ser.* **130** no. 2, (Oct., 2000) 339–350, arXiv:astro-ph/9911292 [astro-ph].

[34] R. M. Crocker, F. Melia, and R. R. Volkas, "Searching for Long-Wavelength Neutrino Oscillations in the Distorted Neutrino Spectrum of Galactic Supernova Remnants," *Astrophys. J. Suppl. Ser.* **141** no. 1, (July, 2002) 147–155, arXiv:astro-ph/0106090 [astro-ph].

[35] J. F. Beacom, N. F. Bell, D. Hooper, J. G. Learned, S. Pakvasa, and T. J. Weiler, "PseudoDirac neutrinos: A Challenge for neutrino telescopes," *Phys. Rev. Lett.* **92** (2004) 011101, arXiv:hep-ph/0307151.

[36] P. Keranen, J. Maalampi, M. Myyrylainen, and J. Riittinen, "Effects of sterile neutrinos on the ultrahigh-energy cosmic neutrino flux," *Phys. Lett. B* **574** (2003) 162–168, arXiv:hep-ph/0307041.

[37] A. Esmaili, "Pseudo-Dirac Neutrino Scenario: Cosmic Neutrinos at Neutrino Telescopes," *Phys. Rev. D* **81** (2010) 013006, arXiv:0909.5410 [hep-ph].

[38] A. Esmaili and Y. Farzan, "Implications of the Pseudo-Dirac Scenario for Ultra High Energy Neutrinos from GRBs," *JCAP* **12** (2012) 014, arXiv:1208.6012 [hep-ph].

[39] I. M. Shoemaker and K. Murase, "Probing BSM Neutrino Physics with Flavor and Spectral Distortions: Prospects for Future High-Energy Neutrino Telescopes," *Phys. Rev. D* **93** no. 8, (2016) 085004, arXiv:1512.07228 [astro-ph.HE].

[40] V. Brdar and R. S. L. Hansen, "IceCube Flavor Ratios with Identified Astrophysical Sources: Towards Improving New Physics Testability," *JCAP* **02** (2019) 023, arXiv:1812.05541 [hep-ph].

[41] Y. F. Perez-Gonzalez and M. Sen, "From Dirac to Majorana: The cosmic neutrino background capture rate in the minimally extended Standard Model," *Phys. Rev. D* **109** no. 2, (2024) 023022, arXiv:2308.05147 [hep-ph].

[42] Z. Chen, J. Liao, J. Ling, and B. Yue, "Constraining super-light sterile neutrinos at Borexino and KamLAND," *JHEP* **09** (2022) 004, arXiv:2205.07574 [hep-ph].

[43] R. Barbieri and A. Dolgov, "Bounds on Sterile-neutrinos from Nucleosynthesis," *Phys. Lett. B* **237** (1990) 440–445.

[44] K. Enqvist, K. Kainulainen, and J. Maalampi, "Resonant neutrino transitions and nucleosynthesis," *Phys. Lett. B* **249** (1990) 531–534.

[45] **IceCube** Collaboration, R. Abbasi *et al.*, "Evidence for neutrino emission from the nearby active galaxy NGC 1068," *Science* **378** no. 6619, (2022) 538–543,

arXiv:2211.09972 [astro-ph.HE].
[46] T. Rink and M. Sen, "Constraints on pseudo-Dirac neutrinos using high-energy neutrinos from NGC 1068," *Phys. Lett. B* **851** (2024) 138558, arXiv:2211.16520 [hep-ph].
[47] K. Dixit, L. S. Miranda, and S. Razzaque, "Searching for Pseudo-Dirac neutrinos from Astrophysical sources in IceCube data," arXiv:2406.06476 [astro-ph.HE].
[48] **IceCube** Collaboration, M. G. Aartsen *et al.*, "Observation of the cosmic-ray shadow of the Moon with IceCube," *Phys. Rev. D* **89** no. 10, (2014) 102004, arXiv:1305.6811 [astro-ph.HE].
[49] **IceCube** Collaboration, R. Abbasi *et al.*, "IceCube Data for Neutrino Point-Source Searches Years 2008-2018," (1, 2021) , arXiv:2101.09836 [astro-ph.HE].
[50] **IceCube** Collaboration, M. G. Aartsen *et al.*, "Search for astrophysical sources of neutrinos using cascade events in IceCube," *Astrophys. J.* **846** no. 2, (2017) 136, arXiv:1705.02383 [astro-ph.HE].
[51] **KM3Net** Collaboration, S. Adrian-Martinez *et al.*, "Letter of intent for KM3NeT 2.0" *J. Phys. G* **43** no. 8, (2016) 084001, arXiv:1601.07459 [astro-ph.IM].
[52] **KM3NeT** Collaboration, T. van Eeden, J. Seneca, and A. Heijboer, "High-energy reconstruction for single and double cascades using the KM3NeT detector," *PoS* **ICRC2021** (2021) 1089, arXiv:2205.02641 [astro-ph.IM].
[53] N. Song, S. W. Li, C. A. Argüelles, M. Bustamante, and A. C. Vincent, "The Future of High-Energy Astrophysical Neutrino Flavor Measurements," *JCAP* **04** (2021) 054, arXiv:2012.12893 [hep-ph].
[54] **IceCube-Gen2** Collaboration, M. G. Aartsen *et al.*, "IceCube-Gen2: the window to the extreme Universe," *J. Phys. G* **48** no. 6, (2021) 060501, arXiv:2008.04323 [astro-ph.HE].
[55] V. A. Allakhverdyan *et al.*, "Deep-Water Neutrino Telescope in Lake Baikal," *Phys. Atom. Nucl.* **84** no. 9, (2021) 1600–1609.
[56] **P-ONE** Collaboration, M. Agostini *et al.*, "The Pacific Ocean Neutrino Experiment," *Nature Astron.* **4** no. 10, (2020) 913–915, arXiv:2005.09493 [astro-ph.HE].
[57] Z. P. Ye *et al.*, "A multi-cubic-kilometre neutrino telescope in the western Pacific Ocean," arXiv:2207.04519 [astro-ph.HE].
[58] **TAMBO** Collaboration, W. G. Thompson, "TAMBO: Searching for Tau Neutrinos in the Peruvian Andes," in *38th International Cosmic Ray Conference*. 8, 2023. arXiv:2308.09753 [astro-ph.HE].
[59] A. N. Otte, A. M. Brown, M. Doro, A. Falcone, J. Holder, E. Judd, P. Kaaret, M. Mariotti, K. Murase, and I. Taboada, "Trinity: An Air-Shower Imaging Instrument to detect Ultrahigh Energy Neutrinos," arXiv:1907.08727 [astro-ph.IM].
[60] **Radar Echo Telescope** Collaboration, S. Prohira *et al.*, "Toward High Energy Neutrino Detection with the Radar Echo Telescope for Cosmic Rays (RET-CR)," *PoS* **ICRC2021** (2021) 1082.
[61] S. L. Glashow, "Resonant Scattering of Antineutrinos," *Phys. Rev.* **118** (1960) 316–317.
[62] **IceCube** Collaboration, M. G. Aartsen *et al.*, "Detection of a particle shower at the Glashow resonance with IceCube," *Nature* **591** no. 7849, (2021) 220–224, arXiv:2110.15051 [hep-ex]. [Erratum: Nature 592, E11 (2021)].
[63] J. G. Learned and S. Pakvasa, "Detecting tau-neutrino oscillations at PeV energies," *Astropart. Phys.* **3** (1995) 267–274, arXiv:hep-ph/9405296 [hep-ph].
[64] J. P. Rachen and P. Meszaros, "Photohadronic neutrinos from transients in astrophysical sources," *Phys. Rev. D* **58** (1998) 123005, arXiv:astro-ph/9802280.
[65] T. Kashti and E. Waxman, "Flavoring astrophysical neutrinos: Flavor ratios depend on energy," *Phys. Rev. Lett.* **95** (2005) 181101, arXiv:astro-ph/0507599.
[66] M. Kachelriess, S. Ostapchenko, and R. Tomas, "High energy neutrino yields from astrophysical sources. 2. Magnetized sources," *Phys. Rev. D* **77** (2008) 023007, arXiv:0708.3047 [astro-ph].
[67] S. Hummer, M. Maltoni, W. Winter, and C. Yaguna, "Energy dependent neutrino flavor ratios from cosmic accelerators on the Hillas plot," *Astropart. Phys.* **34** (2010) 205–224, arXiv:1007.0006 [astro-ph.HE].
[68] W. Winter, "Describing the Observed Cosmic Neutrinos by Interactions of Nuclei with Matter," *Phys. Rev. D* **90** no. 10, (2014) 103003, arXiv:1407.7536 [astro-ph.HE].
[69] L. A. Anchordoqui, H. Goldberg, F. Halzen, and T. J. Weiler, "Galactic point sources of TeV antineutrinos," *Phys. Lett. B* **593** (2004) 42, arXiv:astro-ph/0311002.
[70] L. A. Anchordoqui, "Neutron β-decay as the origin of IceCube's PeV (anti)neutrinos," *Phys. Rev. D* **91** (2015) 027301, arXiv:1411.6457 [astro-ph.HE].
[71] P. Lipari, M. Lusignoli, and D. Meloni, "Flavor Composition and Energy Spectrum of Astrophysical Neutrinos," *Phys. Rev. D* **75** (2007) 123005, arXiv:0704.0718 [astro-ph].
[72] O. Mena, S. Palomares-Ruiz, and A. C. Vincent, "Flavor Composition of the High-Energy Neutrino Events in IceCube," *Phys. Rev. Lett.* **113** (2014) 091103, arXiv:1404.0017 [astro-ph.HE].
[73] A. Palladino, G. Pagliaroli, F. L. Villante, and F. Vissani, "What is the Flavor of the Cosmic Neutrinos Seen by IceCube?," *Phys. Rev. Lett.* **114** no. 17, (2015) 171101, arXiv:1502.02923 [astro-ph.HE].
[74] M. Bustamante, J. F. Beacom, and W. Winter, "Theoretically palatable flavor combinations of astrophysical neutrinos," *Phys. Rev. Lett.* **115** no. 16, (2015) 161302, arXiv:1506.02645 [astro-ph.HE].
[75] M. Bustamante and M. Ahlers, "Inferring the flavor of high-energy astrophysical neutrinos at their sources," *Phys. Rev. Lett.* **122** no. 24, (2019) 241101, arXiv:1901.10087 [astro-ph.HE].
[76] A. Palladino, "The flavor composition of astrophysical neutrinos after 8 years of IceCube: an indication of neutron decay scenario?," *Eur. Phys. J. C* **79** no. 6, (2019) 500, arXiv:1902.08630 [astro-ph.HE].
[77] Q. Liu, D. F. G. Fiorillo, C. A. Argüelles, M. Bustamante, N. Song, and A. C. Vincent, "Identifying Energy-Dependent Flavor Transitions in High-Energy Astrophysical Neutrino Measurements," arXiv:2312.07649 [astro-ph.HE].
[78] P. S. B. Dev, S. Jana, and Y. Porto, "Flavor Matters, but Matter Flavors: Matter Effects on Flavor

Composition of Astrophysical Neutrinos," arXiv:2312.17315 [hep-ph].
[79] L. Wolfenstein, "Neutrino Oscillations in Matter," *Phys. Rev. D* **17** (1978) 2369–2374.
[80] S. P. Mikheyev and A. Y. Smirnov, "Resonance Amplification of Oscillations in Matter and Spectroscopy of Solar Neutrinos," *Sov. J. Nucl. Phys.* **42** (1985) 913–917.
[81] **Particle Data Group** Collaboration, R. L. Workman *et al.*, "Review of Particle Physics," *PTEP* **2022** (2022) 083C01.
[82] I. Esteban, M. C. Gonzalez-Garcia, M. Maltoni, T. Schwetz, and A. Zhou, "The fate of hints: updated global analysis of three-flavor neutrino oscillations," *JHEP* **09** (2020) 178, arXiv:2007.14792 [hep-ph].
[83] **NuFIT** Collaboration, "Three-neutrino fit based on data available in march 2024." www.nu-fit.org.
[84] C. Giganti, "T2k recent results and plans." https://agenda.infn.it/event/37867/contributions/233954/attachments/121809/177671/Neutrino2024_T2K_Claudio.pdf. Talk given at Neutrino 2024 (June 17, 2024).
[85] J. Wolcott, "New nova results with 10 years of data." https://agenda.infn.it/event/37867/contributions/233955/attachments/121832/177712/2024-06-17%20Wolcott%20NOvA%202024%20results%20-%20NEUTRINO.pdf. Talk given at Neutrino 2024 (June 17, 2024).
[86] K. J. Kelly, P. A. N. Machado, S. J. Parke, Y. F. Perez-Gonzalez, and R. Z. Funchal, "Neutrino mass ordering in light of recent data," *Phys. Rev. D* **103** no. 1, (2021) 013004, arXiv:2007.08526 [hep-ph].
[87] V. B. Valera, D. F. G. Fiorillo, I. Esteban, and M. Bustamante, "New limits on neutrino decay from high-energy astrophysical neutrinos," arXiv:2405.14826 [astro-ph.HE].
[88] B. Batell and W. Yin, "Cosmic Stability of Dark Matter from Pauli Blocking," arXiv:2406.17028 [hep-ph].
[89] J. M. Berryman *et al.*, "Neutrino self-interactions: A white paper," *Phys. Dark Univ.* **42** (2023) 101267, arXiv:2203.01955 [hep-ph].
[90] T. Dalton, S. L. Morris, and M. Fumagalli, "Probing the physical properties of the intergalactic medium using gamma-ray bursts," *Mon. Not. Roy. Astron. Soc.* **502** no. 4, (2021) 5981–5996, arXiv:2102.02530 [astro-ph.CO].
[91] **Planck** Collaboration, N. Aghanim *et al.*, "Planck 2018 results. VI. Cosmological parameters," *Astron. Astrophys.* **641** (2020) A6, arXiv:1807.06209 [astro-ph.CO]. [Erratum: Astron.Astrophys. 652, C4 (2021)].
[92] A. M. Hopkins and J. F. Beacom, "On the normalisation of the cosmic star formation history," *Astrophys. J.* **651** (2006) 142–154, arXiv:astro-ph/0601463.
[93] H. Yuksel, M. D. Kistler, J. F. Beacom, and A. M. Hopkins, "Revealing the High-Redshift Star Formation Rate with Gamma-Ray Bursts," *Astrophys. J. Lett.* **683** (2008) L5–L8, arXiv:0804.4008 [astro-ph].
[94] **IceCube** Collaboration, R. Abbasi *et al.*, "Observation of high-energy neutrinos from the Galactic plane," *Science* **380** no. 6652, (2023) adc9818, arXiv:2307.04427 [astro-ph.HE].
[95] **KATRIN** Collaboration, M. Aker *et al.*, "New Constraint on the Local Relic Neutrino Background Overdensity with the First KATRIN Data Runs," *Phys. Rev. Lett.* **129** no. 1, (2022) 011806, arXiv:2202.04587 [nucl-ex].
[96] V. Brdar, P. S. B. Dev, R. Plestid, and A. Soni, "A new probe of relic neutrino clustering using cosmogenic neutrinos," *Phys. Lett. B* **833** (2022) 137358, arXiv:2207.02860 [hep-ph].
[97] M. Bauer and J. D. Shergold, "Limits on the cosmic neutrino background," *JCAP* **01** (2023) 003, arXiv:2207.12413 [hep-ph].
[98] Y.-D. Tsai, J. Eby, J. Arakawa, D. Farnocchia, and M. S. Safronova, "OSIRIS-REx constraints on local dark matter and cosmic neutrino profiles," *JCAP* **02** (2024) 029, arXiv:2210.03749 [hep-ph].
[99] M. Císcar-Monsalvatje, G. Herrera, and I. M. Shoemaker, "Upper Limits on the Cosmic Neutrino Background from Cosmic Rays," arXiv:2402.00985 [hep-ph].
[100] J. Franklin, I. Martinez-Soler, Y. F. Perez-Gonzalez, and J. Turner, "Constraints on the Cosmic Neutrino Background from NGC 1068," arXiv:2404.02202 [hep-ph].
[101] A. G. De Marchi, A. Granelli, J. Nava, and F. Sala, "Relic Neutrino Background from Cosmic-Ray Reservoirs," arXiv:2405.04568 [hep-ph].
[102] G. Herrera, S. Horiuchi, and X. Qi, "Diffuse Boosted Cosmic Neutrino Background," arXiv:2405.14946 [hep-ph].
[103] A. Ringwald and Y. Y. Y. Wong, "Gravitational clustering of relic neutrinos and implications for their detection," *JCAP* **12** (2004) 005, arXiv:hep-ph/0408241.
[104] P. Mertsch, G. Parimbelli, P. F. de Salas, S. Gariazzo, J. Lesgourgues, and S. Pastor, "Neutrino clustering in the Milky Way and beyond," *JCAP* **01** (2020) 015, arXiv:1910.13388 [astro-ph.CO].
[105] F. Zimmer, C. A. Correa, and S. Ando, "Influence of local structure on relic neutrino abundances and anisotropies," *JCAP* **11** (2023) 038, arXiv:2306.16444 [astro-ph.CO].
[106] W. Elbers, C. S. Frenk, A. Jenkins, B. Li, S. Pascoli, J. Jasche, G. Lavaux, and V. Springel, "Where shadows lie: reconstruction of anisotropies in the neutrino sky," *JCAP* **10** (2023) 010, arXiv:2307.03191 [astro-ph.CO].
[107] E. B. Holm, S. Zentarra, and I. M. Oldengott, "Local clustering of relic neutrinos: Comparison of kinetic field theory and the Vlasov equation," arXiv:2404.11295 [hep-ph].
[108] A. Y. Smirnov and X.-J. Xu, "Neutrino bound states and bound systems," *JHEP* **08** (2022) 170, arXiv:2201.00939 [hep-ph].
[109] K. Fang, J. S. Gallagher, and F. Halzen, "The TeV Diffuse Cosmic Neutrino Spectrum and the Nature of Astrophysical Neutrino Sources," *Astrophys. J.* **933** no. 2, (2022) 190, arXiv:2205.03740 [astro-ph.HE].
[110] P. D. Serpico and G. G. Raffelt, "Lepton asymmetry and primordial nucleosynthesis in the era of precision cosmology," *Phys. Rev. D* **71** (2005) 127301, arXiv:astro-ph/0506162.
[111] A.-K. Burns, T. M. P. Tait, and M. Valli, "Indications for a Nonzero Lepton Asymmetry from Extremely

Metal-Poor Galaxies," *Phys. Rev. Lett.* **130** no. 13, (2023) 131001, arXiv:2206.00693 [hep-ph].

[112] M. Escudero, A. Ibarra, and V. Maura, "Primordial lepton asymmetries in the precision cosmology era: Current status and future sensitivities from BBN and the CMB," *Phys. Rev. D* **107** no. 3, (2023) 035024, arXiv:2208.03201 [hep-ph].

[113] **IceCube** Collaboration, R. Abbasi *et al.*, "Observation of Seven Astrophysical Tau Neutrino Candidates with IceCube," *Phys. Rev. Lett.* **132** no. 15, (2024) 151001, arXiv:2403.02516 [astro-ph.HE].

[114] **IceCube** Collaboration, M. G. Aartsen *et al.*, "A combined maximum-likelihood analysis of the high-energy astrophysical neutrino flux measured with IceCube," *Astrophys. J.* **809** no. 1, (2015) 98, arXiv:1507.03991 [astro-ph.HE].

[115] **IceCube** Collaboration, D. Cowen *et al.*, "Summary of IceCube tau neutrino searches and flavor composition measurements of the diffuse astrophysical neutrino flux," *PoS* **ICRC2023** (2023) 1122.

[116] M. Ackermann *et al.*, "High-energy and ultra-high-energy neutrinos: A Snowmass white paper," *JHEAp* **36** (2022) 55–110, arXiv:2203.08096 [hep-ph].

[117] **IceCube-Gen2** Collaboration, R. Abbasi *et al.*, "Sensitivity of IceCube-Gen2 to measure flavor composition of Astrophysical neutrinos," *PoS* **ICRC2023** (2023) 1123.

[118] **JUNO** Collaboration, F. An *et al.*, "Neutrino Physics with JUNO," *J. Phys. G* **43** no. 3, (2016) 030401, arXiv:1507.05613 [physics.ins-det].

[119] **DUNE** Collaboration, R. Acciarri *et al.*, "Long-Baseline Neutrino Facility (LBNF) and Deep Underground Neutrino Experiment (DUNE): Conceptual Design Report, Volume 2: The Physics Program for DUNE at LBNF," arXiv:1512.06148 [physics.ins-det].

[120] **Hyper-Kamiokande** Collaboration, K. Abe *et al.*, "Hyper-Kamiokande Design Report," arXiv:1805.04163 [physics.ins-det].

[121] C. S. Fong and Y. Porto, "Constraining pseudo-Diracness with astrophysical neutrino flavors," arXiv:2406.15566 [hep-ph].